THE ASTROPHYSICAL JOURNAL, 453:139–153, 1995 November 1

THE INTERACTION BETWEEN SPIRAL GALAXIES IC 2163 AND NGC 2207. II. MODELS

BRUCE G. ELMEGREEN,[1] MARIA SUNDIN,[2] MICHELE KAUFMAN,[3] ELIAS BRINKS,[4] AND DEBRA MELOY ELMEGREEN[5]

Received 1994 November 28; accepted 1995 May 2

ABSTRACT

Observations of the disturbed morphologies and internal velocity distributions, and of the relative positions, orientations, and centroid velocities of the interacting spiral galaxies IC 2163 and NGC 2207, are reproduced by computer simulations of each galaxy. The ocular morphology of IC 2163, consisting of a bright oval with pointed apices and a double-parallel structure in the tidal arm, as well as the streaming motions along the oval and the arms and the nearly perpendicular alignment of the kinematic and photometric minor axes, are fitted to a model in which IC 2163 is reacting to an in-plane, prograde encounter with NGC 2207 that had a closest approach $\sim 4 \times 10^7$ yr ago. In NGC 2207, strong velocity anomalies consisting of a global distortion of the velocity distribution into an S shape and a 40° misalignment of the kinematic and photometric minor axes are fitted by a dynamical model in which the companion, IC 2163, moved in a plane perpendicular to the disk of NGC 2207 with the same relative orbit as in the IC 2163 model. The resulting out-of-plane tidal forces are producing a warp of the disk of NGC 2207 with present z-displacements as large as 9 kpc and present z-velocities up to 100 km s^{-1}. The large southern extension of NGC 2207 observed in H I and in optical images is probably a tidal remnant from the time, $\sim 2.4 \times 10^8$ yr ago, when IC 2163 crossed the western extrapolated plane of NGC 2207 from the near side to the far side, prior to perigalacticon on the far side. The high resolution of both the observations and the models gives an unprecedented view of the dynamics of strong tidal interactions between galaxies.

Subject headings: galaxies: individual (IC 2163, NGC 2207) — galaxies: interactions — galaxies: kinematics and dynamics — galaxies: structure — radio continuum: galaxies

1. INTRODUCTION

Optical, H I, and radio continuum observations of the interacting spiral galaxies NGC 2207 and IC 2163 were presented by Elmegreen et al. (1994, hereafter Paper I). IC 2163 has a sharply pointed central oval that continues smoothly on each side to form long tidal arms. Such "ocular" structure was shown previously to result from a prograde, in-plane encounter with a companion of equal mass (Elmegreen et al. 1991, hereafter ESES; Donner, Engstrom, & Sundelius et al. 1991; Sundin 1993). In optical images (see Fig. 1 in Paper I), NGC 2207 shows only a slight deformation associated with a faint extension of blue light toward the south.

Here we use our observations to constrain the possible orbits for the two galaxies and to model each one in detail. The models explain the following main features (see Paper I): the ocular structure and double-parallel arm in IC 2163, including the observed streaming motions on the oval and tidal arms, the nearly perpendicular alignment of the kinematic minor axis and the photometric minor axis in IC 2163, the apparent bar in IC 2163, the S-shaped velocity contours throughout NGC 2207, the 40° offset between the kinematic and photometric minor axes in NGC 2207, and the current positions, relative velocities, and orientations of the galaxies in space.

The large offsets between the kinematic and photometric minor axes in these galaxies require internal dynamics that are strongly perturbed. Our models suggest that the offset in IC 2163 is the result of an intrinsically oval shape of the main disk and central eyelid feature, and that the offset and S-shaped velocity distribution in NGC 2207 result from a large warp.

The observations of IC 2163 and NGC 2207 are sufficiently detailed that we are able to understand the orbital and interaction dynamics by fitting the data to galaxy encounter simulations that have high spatial resolution. We use consistent relative orbits for the two galaxies but fit only one galaxy at a time. Thus, the observed features in IC 2163 are fitted by a highly resolved, two-dimensional model of that galaxy alone, treating the companion galaxy NGC 2207 as a point mass. Similarly, the observed features in NGC 2207 are fitted by another highly resolved two-coordinate model of NGC 2207 alone, treating IC 2163 as a point mass. In the first case, the two dimensions are those of the galactic plane in IC 2163, and the computer code is a conventional N-body Fourier transform code for a two-dimensional stellar disk (from Thomasson 1989). In the second case, the two coordinates for the computation are the azimuthal coordinate and the perpendicular-to-plane coordinate (in a three-dimensional geometry that assumes no radial motions) for NGC 2207 as IC 2163 passes nearly straight over its pole. The self-gravity in this model (perpendicular to the plane) is determined by an N^2 summation over all pairs of disk segments. These two-coordinate calculations provide exceptionally good fits to the galaxies because of a fortunate alignment of the plane of the NGC 2207 orbit nearly parallel to the disk of IC 2163 and of the plane of the IC 2163 orbit nearly perpendicular to the disk of NGC

[1] IBM Research Division, T. J. Watson Research Center, P.O. Box 218, Yorktown Heights, NY 10598.
[2] Department of Astronomy/Astrophysics, Chalmers University of Technology, S-412 96 Göteborg, Sweden.
[3] Department of Physics, Ohio State University, 174 West 18th Avenue, Columbus, OH 43210.
[4] National Radio Astronomy Observatory, P.O. Box O, Socorro, NM 87801. (The National Radio Astronomy Observatory is operated by Associated Universities, Inc., under cooperative agreement with the National Science Foundation.)
[5] Vassar College Observatory, Poughkeepsie, NY 12601.

2207. Such a simplifying strategy is not generally useful, however, because other interacting galaxies are likely to be much more complex, with simultaneous in-plane and out-of-plane motions. Indeed, three-dimensional studies of galaxy pairs generally show complex dynamics (see review in Barnes & Hernquist 1992), and previous attempts to fit such models to observations (Stanford & Balcells 1991; Smith & Wallin 1992; Salo & Laurikainen 1993) have not considered the level of detail that is available here.

The high velocity dispersions in the H I gas in both IC 2163 and NGC 2207 (Paper I) presumably arise from enhanced turbulent motions. Such dispersions are not fitted here, but they were modeled in a separate study of interacting galaxies, based on the present observations (Elmegreen, Kaufman, & Thomasson 1993). Our model for NGC 2207 also considers no radial motions, so it does not explain the large southern extension. This type of feature usually results from the asymmetry in a tidal force at close range; i.e., the nearby part of the disk is drawn toward the companion more strongly than the far side is drawn away (Lynds & Toomre 1976). Aside from these two features (the high velocity dispersion and the southern extension), essentially all of the large-scale structural and velocity anomalies that were observed in these galaxies are reproduced by the simulations in a self-consistent way.

In § 2, the main orbital constraints provided by the observations are considered. In §§ 3 and 4, the IC 2163 and NGC 2207 models are presented and compared with the observed features. The results are summarized in § 5.

2. CONSTRAINTS ON THE ORBITS

In our interpretation, there were two main events that led to the observed structural and kinematic disturbances in these galaxies. The first occurred several hundred million years ago and was responsible for the southern H I extension in NGC 2207. The southern extension in NGC 2207 is not exactly on the companion side of the disk at the present time; this shift in position is a useful clue about the history of the orbit. This feature must be older than the ocular structure in IC 2163 because the angular and expansion velocities of the outer disk of NGC 2207 are much slower than the angular velocities near the oval of IC 2163. The timescale for the formation of the southern extension is on the order of one-half of the rotation time for the outer part of NGC 2207. A similar expansion of part of a galactic disk away from the main disk was found for another interacting pair by Moles et al. (1994).

The second major event occurred within a half-rotation of the inner oval region of IC 2163, or some 40 million years ago. This event generated the ocular structure in IC 2163, the high H I velocity dispersions in both galaxies, and the S-shaped distortion of the velocity field in NGC 2207. All of these features are relatively short-lived.

Because of the nature of the interaction dynamics, the first event, leading to the southern extension, was probably a distant, high-inclination passage of IC 2163 through the extrapolated plane of NGC 2207, and the second event was probably the closest approach between the two galactic nuclei. Timing constraints imply that both events took place on the same orbital flyby; otherwise, the southern extension would have sheared away too much.

To specify the orbit more precisely, we need to know the orientations of the galaxies in space. For trailing spiral arms, NGC 2207 must be spinning clockwise and IC 2163 counterclockwise. The near side (to us) of IC 2163 is in the north by northwest, on the kinematic minor axis at position angle 335°. Although streaming motions introduce an uncertainty in the position angle, the model in § 3 is consistent with this orientation. The near side of NGC 2207 could be anywhere between position angles $\sim 20°$ (photometric minor axis) and $\sim 60°$ (kinematic minor axis). Since IC 2163 is partially behind NGC 2207, the side of IC 2163 that is closest to NGC 2207 in space is the same side that is closest in projection on the sky, i.e., the northwestern side of IC 2163. Then, the eastern double-parallel arm in IC 2163 is on the side farthest from its companion, as predicted by the models.

A schematic diagram of the positions of the two galaxies is shown in Figure 1. The bottom right diagram is the sky view. The top diagrams are the galaxy pair viewed from above, with Earth downward in the figure. The top left and right diagrams are identical except that on the top left, the region of the radio continuum ridge in NGC 2207 is indicated by a curved box. The bottom left diagram is the galaxy pair viewed from the left side, with Earth far away on the right. Figure 1 assumes that the inclinations of both galaxies are 40° (the model gives 35° for NGC 2207), that the position angles for the line of nodes in IC 2163 and NGC 2207 are 65° and 110°, respectively, that each disk is flat (which is incorrect for NGC 2207), and that the intrinsic galaxy shapes are circular for NGC 2207 and elliptical with an axis ratio of 2:1 for IC 2163. In § 4, we show how the warp in NGC 2207 changes the position angle of the ellipse, making the intrinsic line of nodes at $\sim 140°$ instead of 110°. For Figure 1, the relative positions of the two galaxies in the plane of the sky were chosen to agree with the observations, and in depth they were chosen to have their centers spaced by a distance equal to 0.6 of the radius of NGC 2207 (as in the preferred model at the present epoch). The solid portions of each projected ellipse represent the edges that are closest to the observer from that perspective, i.e., closest to Earth for the sky perspective, most northern for the top perspective, and most eastern for the side perspective. The tidal arms in IC 2163 are not drawn.

Figure 1 helps us visualize the interaction between these two galaxies, which is also constrained by the morphology, kinematics, and sense of rotation from the spirals. The ocular shape and double-parallel arm in IC 2163 implies that NGC 2207 moved in a prograde sense relative to the rotation of the disk of IC 2163 and in an orbit that lies fairly close to the plane of IC 2163. Thus, in Figure 1, the side of IC 2163 nearest Earth is pointing toward the center of NGC 2207, which implies that NGC 2207 is currently in the plane of IC 2163. Moving parallel to its own disk, IC 2163 must have traveled along the backside of NGC 2207 in a counterclockwise sense from approximately the northwest to its present position partially behind the eastern edge of NGC 2207.

Because the centroid velocities of the two galaxies are nearly the same, the main component of the orbital velocity of each galaxy is now in the plane of the sky. This eliminates orbits in which IC 2163 is approaching (or has just passed through) the disk of NGC 2207 at a shallow angle to the line of sight.

Considering this backside motion, the earliest event mentioned above, connected with the formation of the southern extension of NGC 2207, must have occurred when IC 2163 passed through the plane of NGC 2207, relatively far from the center, from the front side to the back side. This would have happened several hundred million years ago. This event stretched the adjacent side of NGC 2207 toward IC 2163, and after the outer disk of NGC 2207 rotated, the stretched disk

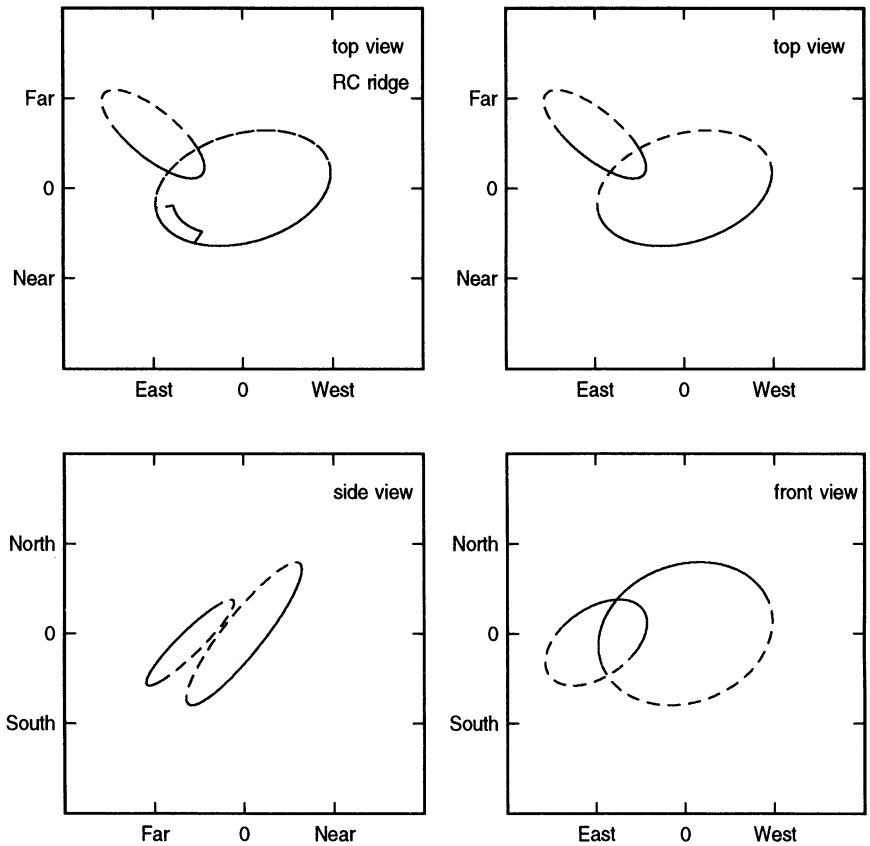

FIG. 1.—Diagram showing probable views of these galaxies from the front (*bottom right*), top, or north (*top right*), and left-hand, or east (*left*), sides in space. Dashed lines indicate parts of the oval that are away from the viewer for that perspective.

became the current southern extension of H I. The position angle of this disk crossing can be estimated from the relative angular speeds of IC 2163 and the outer part of NGC 2207 around the NGC 2207 center. Since the NGC 2207 plane crossing, the average angular speed of IC 2163 around the center of NGC 2207 was probably about the same as the angular speed of the outer part of the NGC 2207 disk around its center. This is because the larger average distance ($\times 2$) of IC 2163 from the center of NGC 2207 is partially offset by the increased average orbit speed ($\times 2^{1/2}$) of IC 2163, which is an equal mass companion, compared to the distance and orbit speed of a typical low-mass star in the outer disk (e.g., 30 kpc) of NGC 2207. Thus, the outer part of the NGC 2207 disk must have turned clockwise over about the same angle as IC 2163 moved counterclockwise around NGC 2207, within a factor of 2. This places the point of disk crossing somewhere in the western quadrant of NGC 2207 (see also Fig. 1), and the time of disk crossing at about one-fourth of the rotation period at ~ 30 kpc in NGC 2207.

The rotation speed of NGC 2207 can be estimated from the universal rotation curve in Persic & Salucci (1991) for spiral galaxies with the same M_B. Although the observed v sin (i) is fairly flat on the major axis of the southern extension with $(v_{obs} - v_{sys}) \sim -100$ km s^{-1} here (see Fig. 21*b* in Paper I), the observed values involve a combination of tangential, radial, and z motions. The Persic & Salucci (1991) value is 220 km s^{-1}, and for this value, with an average radial distance of 30 kpc for the southern extension (which extends approximately from $R_{25} = 22$ kpc to 40 kpc), the disk crossing would have occurred $\sim 2.1 \times 10^8$ yr ago.

A better way to estimate this time would be to consider the motion of gas in the outer part of NGC 2207 if angular momentum is conserved. This gives an angular speed $v_\theta \equiv r\,d\theta/dt = v_0 r_0/r$ for flat rotation curve speed v_0. For an approximately constant radial expansion speed, v_r, $dt = dr/v_r$, so $d\theta/dr = (v_0/v_r)(r_0/r^2)$ and $\Delta\theta = (v_0/v_r)(1 - r_0/r_1)$ for initial and final radii r_0 and r_1. Now assume that the timescale for this expansion is $\Delta t = \Delta r/v_r$ for $\Delta r = r_1 - r_0$. Then, $\Delta t = \Delta\theta r_1/v_0$. If $\Delta\theta \sim \pi/2$ as estimated above, $v_0 = 220$ km s^{-1}, and the final radius is $r_1 = 40$ kpc, then the time since the first disk crossing is $\sim 2.8 \times 10^8$ yr.

Two other features of NGC 2207 follow from the passage of IC 2163 through the extrapolated plane of NGC 2207 2–3 $\times 10^8$ yr ago: the different line of nodes of the southern extension relative to the main optical disk, and the morphology of the filaments there. The main position angle of the southern extension follows from the orbit time of the bulk of the gas since the disk crossing, but the line of nodes of this southern gas, which is clearly different from that of the main disk of NGC 2207, follows from the intrinsically elliptical shape of this disturbance and from the radial variation of its angular velocity around the center. As the tidally stretched gas moved from $R = 20$ kpc to $R = 40$ kpc, its angular velocity would have decreased by the conservation of angular momentum, and it would get systematically shifted counterclockwise relative to the less perturbed material orbiting at smaller radii. This is indeed the sense of the observed shift from the position angle of the main galaxy.

The filaments in the southern extension have a pitch angle in the disk of $50° \pm 20°$ and presumably formed as waves in a

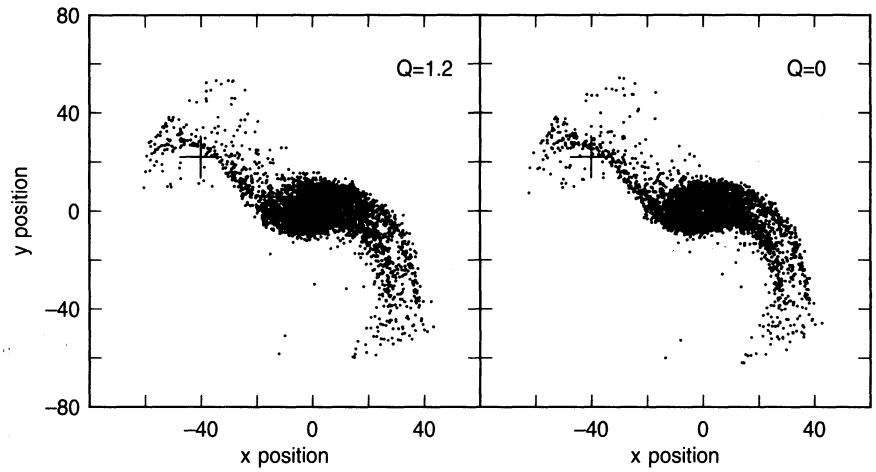

FIG. 2.—Particle plots for two-dimensional N-body simulations of IC 2163, viewed from a face-on perspective. Parameters of the model are discussed in the text. These two models are identical, except that the one on the left has a Q parameter for the stars equal to 1.2, and the one on the right has $Q = 0$ (i.e., a cold stellar disk), to accentuate the double arm on the anticompanion side. The position of the companion is denoted by a plus sign.

shearing and stretching medium. The velocity difference between the inner and outer parts of the filaments in the radial direction is approximately their radial extent of ~ 20 kpc divided by $\sim 2 \times 10^8$ yr since the expansion began, or ~ 100 km s^{-1}. This expansion speed is typical for tidal interactions (e.g., see Lynds & Toomre 1976). The velocity difference between the inner and outer parts of the filaments in the azimuthal direction is $\Delta r r\, d\Omega/dr = (\Delta r/r) \times 220$ km s^{-1} for radial extent Δr, radius r, and circular speed 220 km s^{-1}. This azimuthal velocity difference is ~ 110 km s^{-1} for $\Delta r = 20$ kpc and $r = 40$ kpc, which is comparable to the radial velocity difference over the same radial interval. Thus the pitch angles of the filaments should be arctan $100/110 \sim 42°$, which is reasonably close to the observed value.

3. IC 2163

3.1. *Model*

The morphology of IC 2163 resembles some of the simulations of interacting galaxies shown in ESES, so we ran more models of this type to search for an acceptable fit. Two examples with 4000 plotted particle positions from the model are shown in Figure 2 in face-on views: one with an initial value of the stellar Q equal to 0 (a cold disk) and another with the initial value equal to 1.2. These simulations contain a total of 60,000 star particles in a Kuzmin disk with a Mestel halo, giving a nearly flat rotation curve, as shown in Figure 3 (in model coordinates, see conversion to physical units below). The active disk contains 40% of the total galaxy mass, and the inactive halo contains 60%. There is no bulge or gas. The $Q = 0$ model shows the double arm on the anticompanion side better than the $Q = 1.2$ model, although the latter is more realistic for a stellar disk. The $Q = 0$ model should resemble the gas response in the absence of dissipation. The position of the companion is denoted by a plus sign.

The models in ESES used pure Kuzmin disks, which have falling rotation curves. The Mestel halo gives a better result for IC 2163 because the larger circular velocity at the edge of the disk in the Mestel model makes the pitch angle of the tidal arm as large as it is observed to be. Pure Kuzmin disks give more tightly wrapped tidal arms.

Of all the models we tried, the only interactions that gave the characteristic ocular features in IC 2163 were prograde and in the plane of the galaxy. Retrograde interactions had such short interaction times for the individual disk particles that the companion mass had to be very large to produce a similar disturbance; even then the ocular shape did not appear.

One can define a dimensionless parameter S that is a measure of the perturbation strength as follows:

$$S = \left(\frac{M_c}{M_g}\right)\left(\frac{R_g}{R_c}\right)^3\left(\frac{\Delta T}{T}\right), \quad (1)$$

where M_c and M_g are the companion and galaxy masses, R_g is a convenient measure of the galaxy size (see below), R_c is the distance to the companion at perigalacticon, ΔT is the time it takes the companion to move over an angle of 1 rad relative to the galaxy center at the time of closest approach, and T is the time for stars at R_g to move 1 radian in their orbits. The perturbation strength that reproduces the overall shape and velocity field in IC 2163 is $S \sim 0.12$.

For the purpose of calculating the gravitational force by Fourier transforms, we used a polar grid consisting of 42 radial

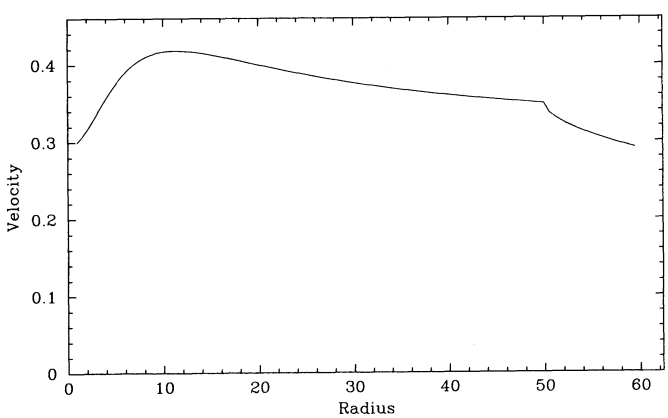

FIG. 3.—Rotation curve for the IC 2163 model shown in Fig. 2. For the physical dimensions discussed in the text, the peak rotation speed corresponds to about 225 km s^{-1}, and the distance unit is 0.45 kpc.

cells and 64 azimuthal cells with an exponential spacing for the radial cells (radius = exp ($2\pi n/64$) for radial cell position n). The galaxy radius R_g equals about R_{25} before the tidal interaction and has approximately the same length as the present semimajor axis of the oval (see examples in ESES). In our model, R_g equals 20 length units and occurs in radial cell $n = 30$. We can calibrate the units of the model by noting that in the best-fit run, the major axis of the oval is about 40 length units (see Fig. 2) at the current epoch. The major axis of the oval in IC 2163 has a plane-of-sky length of about 80″. For the adopted projection shown in Figure 4 below, this corresponds to an unprojected length of about 106″, or 18.1 kpc. Hence, the length unit is 18.1/40 = 0.45 kpc, and R_g is 53″ or 9.1 kpc. The time step in the model is 1/50 of the time for a star orbiting at R_g to move an angular distance of 1 rad. Thus, $T \equiv R_g/V(R_g)$ is 50 time steps. As in § 4.4 in Paper I, we estimate that the unperturbed peak rotation speed in IC 2163 is about 225 km s^{-1}. This gives a time step for the calculation $\delta T = R_g/[50V(R_g)] \approx 0.8 \times 10^6$ yr.

We used $M_c/M_g = 1$ for the figures here (see the discussion of the luminosity ratio in § 2 of Paper I; a slightly larger ratio is easily accounted for in eq. [3] by a smaller R_g/R_c). We adopt an exponential scale length of 29″ and a disk radius of ~50″ before the tidal interaction. Thus, the IC 2163 disk radius was 56% of the current projected separation of 1.′5. The distance of closest approach must be larger than this projected separation. In the best-fit model, we used $R_g/R_c = 20/45.7$ (measured in radial units for the calculation). The pericenter distance, R_c, is not input directly; it has to be determined from the orbit that is part of the interaction solution. The direct inputs are the initial distance of the companion, which was 160 length units, and the orbit type, which was parabolic. With $R_g = 9.1$ kpc, as above, R_c becomes $45.7 \times 9.1/20 = 20.8$ kpc, corresponding to an unprojected distance of 122″ at closest approach. This distance will be used again for the model of NGC 2207 discussed in § 4; it equals 0.95 times the radius R_{25} for NGC 2207. The ratio of times for the simulation shown is $\Delta T/T = 82/50$, measured in the time steps of the simulation.

The output of the models was converted into plots of stellar density and velocity for comparison with the observations. The stellar density distributions were displayed as particle plots and gray scales, and the velocities were converted into gray

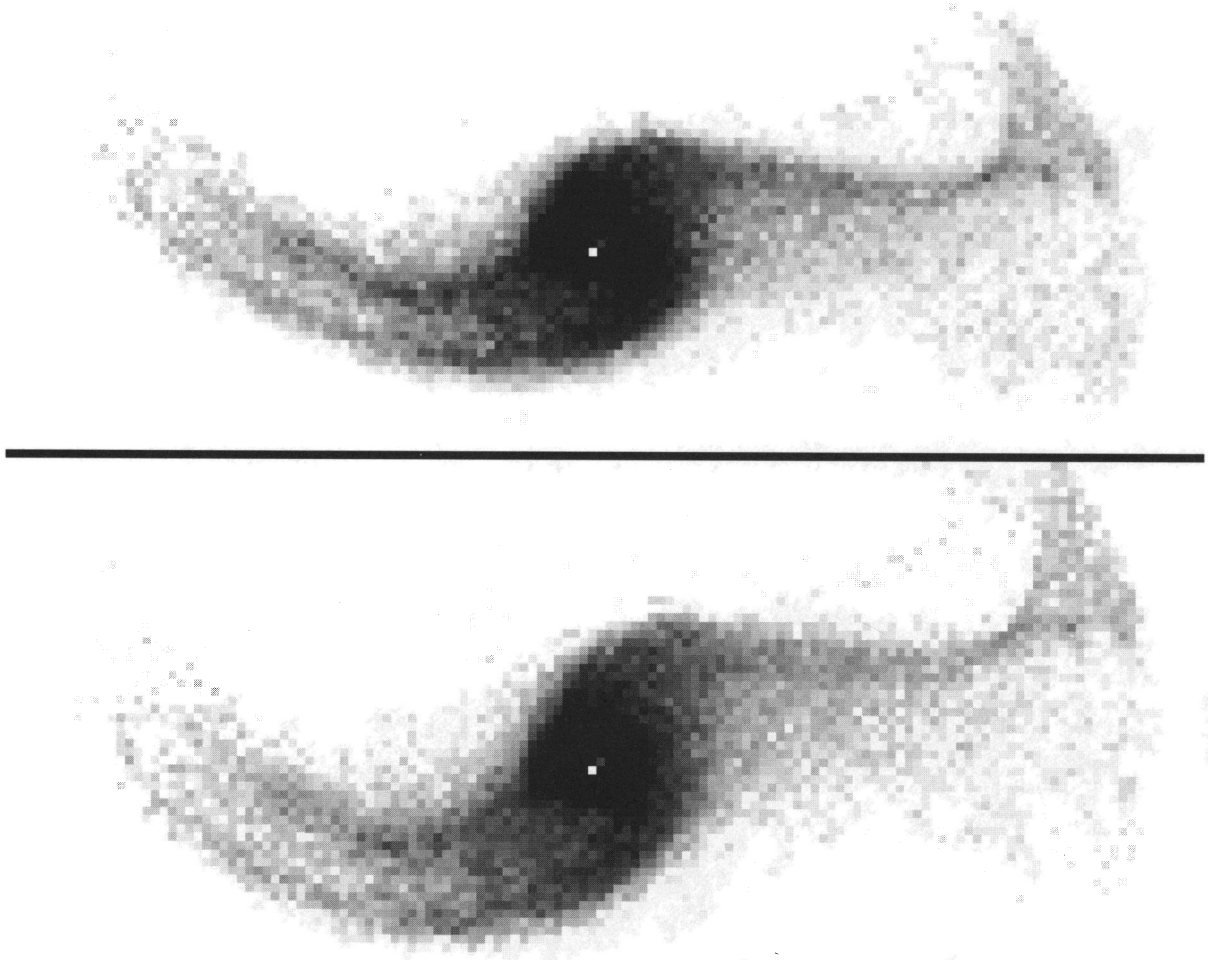

FIG. 4.—The same model as in Fig. 2 with $Q = 1.2$ but shown here with a density gray scale and different projections. *Top*: The model has been rotated first by 200° clockwise, then tilted 40° around the vertical axis, and then rotated 70° counterclockwise. This orientation gives the model the same morphology, kinematic axes, and sky orientation as IC 2163. *Bottom*: The $Q = 1.2$ model is shown without any inclination, but just rotated 130° clockwise around the coordinate system. Note that the nucleus is displaced toward the left of the center of the oval and that this region gives the appearance of a bar oriented to the northwest (*up and to the left*) in the inclined case (*top*). This bar resembles the bar in IC 2163.

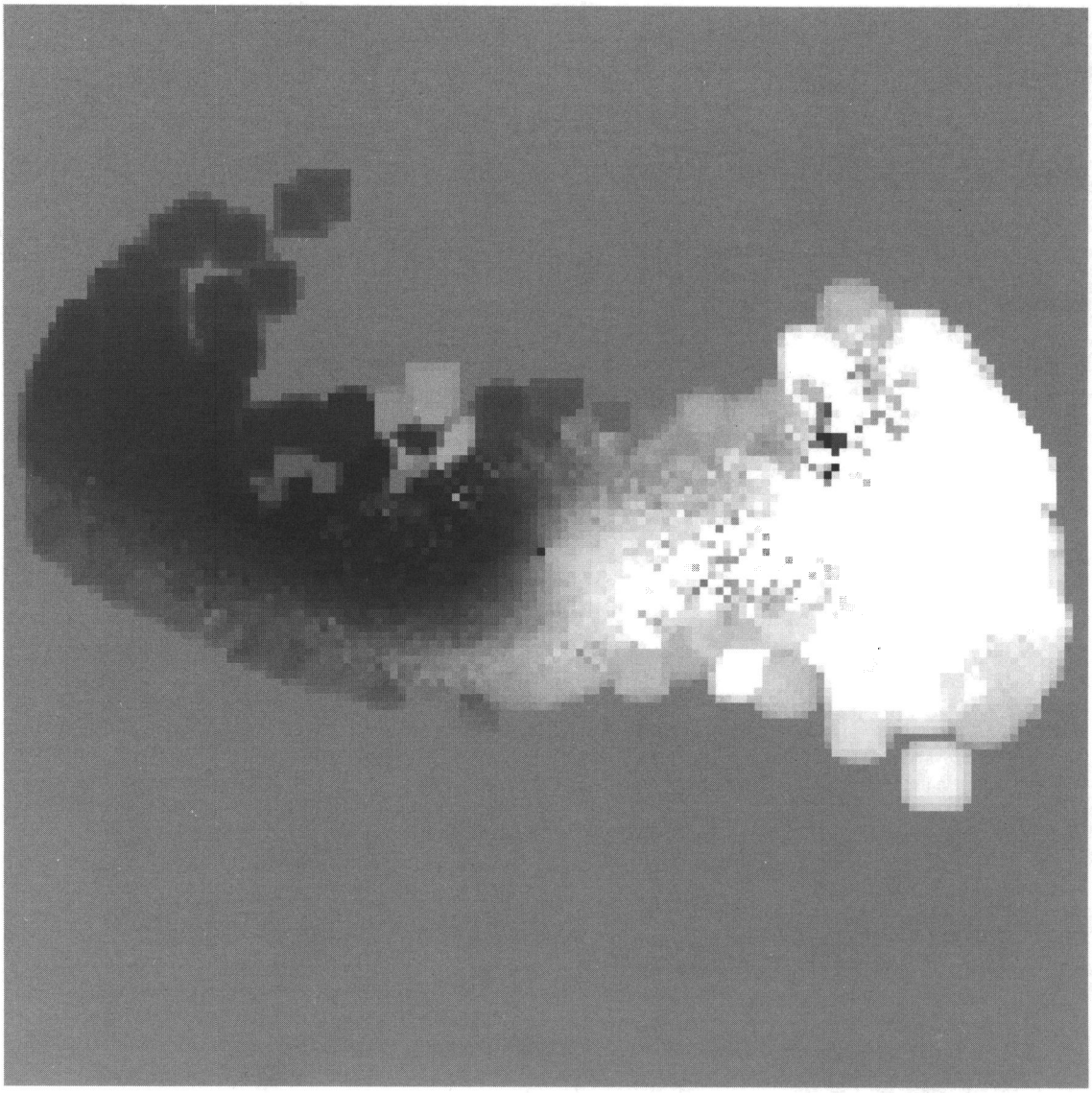

FIG. 5*a*

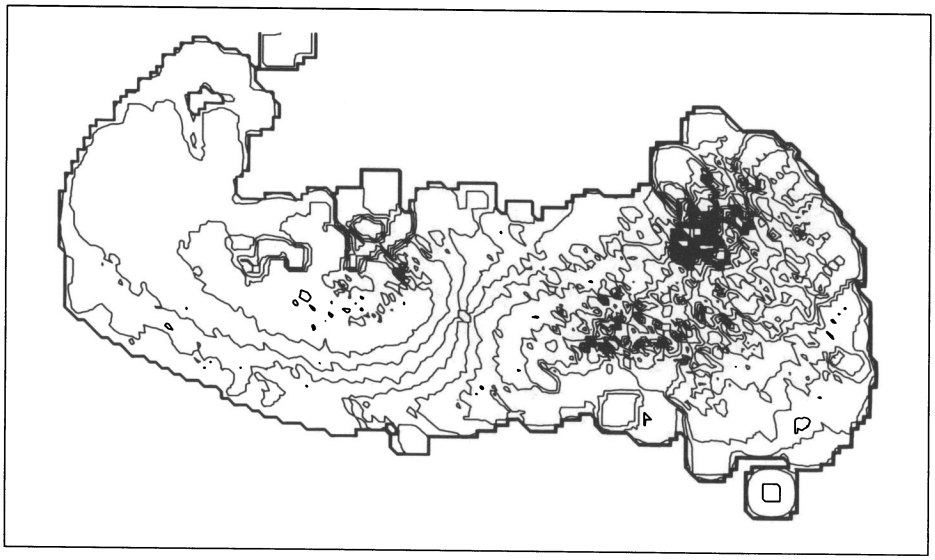

FIG. 5*b*

FIG. 5.—*Top*: Gray-scale representation of the line-of-sight velocity for the preferred orientation in the top of Fig. 4. *Bottom*: Contours for the same line-of-sight velocity distribution. The kinematic major axis in both of these plots is at a position angle of 70° counterclockwise from the vertical in the diagram, as it is in the top frame of Fig. 4.

scales and contours of the line-of-sight component for an assumed orientation. Many different orientations of the model were viewed in this way.

A good fit to IC 2163 is shown on the top in Figure 4. The orientation of the model in this figure was made by first rotating the coordinate system of the model by 200° clockwise, then inclining the model by 40° around the vertical axis, and then rotating the inclined image by 70° counterclockwise. The face-on version, with just a 130° (=200° − 70°) rotation clockwise, is shown at the bottom. Note that the face-on version has a nucleus slightly offset from the center of the oval, as in the observed galaxy IC 2163, and that this offset gives the inclined version a barlike appearance, as in IC 2163. The orientation of the model at the top of Figure 4 is the same as that of IC 2163 with north up.

Figure 5 shows a gray scale and contour diagram of the projected line-of-sight velocity in the model, made with the 200° clockwise rotation, 40° inclination around the vertical, and 70° counterclockwise rotation, as in Figure 4. The major kinematic axis in this figure is at an angle of 70° counterclockwise from the vertical, which corresponds to a kinematic position angle in the sky of 70° from the north.

The inclination of 40°, chosen for the best match of the model to IC 2163, is constrained on the low end by the observed velocity distribution in IC 2163, and on the high end by the morphology of the ocular structure. Inclinations as low as 20° disagree with the observed streaming motions (see § 4.4 in Paper I) and give too small a variation in velocity across the galaxy in the plane-of-sky image. Inclinations as high as 60° make the galaxy too narrow and lose the ocular structure.

The rotation of 200° from the model coordinate system to the direction of the kinematic major axis (clockwise) was chosen mostly on the basis of the shape of the oval. Smaller angles gave too much curvature, and even an upward rise or bump on the top right part of the oval, and larger angles made the top right of the oval too sharply falling. The final rotation of 70° counterclockwise was chosen to make the inclined model look like the images of IC 2163 with north up.

The time step shown in Figures 2, 4, and 5 is 600. Earlier time steps had the double arm too far apart or possible only as a single tidal arm without the streaming arm. Later time steps had the double arm merged into a single tidal arm and the overall tidal arm part much thinner. The time step at the time of closest approach of the companion is 584. Thus the time since the closest approach in the model is 16 time steps, which corresponds to $\sim 1.3 \times 10^7$ yr. Considering that the pericenter distance, the companion mass, and the orbit type (parabolic) are all estimates, and that the real companion is extended and not a point mass, the timing of the collision could be slightly different from this. For example, a good fit to IC 2163 discussed in Paper I, model 89082201, had $M_c/M_g = 1$, $R_c/R_g = 3.75$, and $\Delta T/T = 3.62$ instead of 1, 2.3, and 1.64; the time since closest approach was ~ 100 time steps, or 8×10^7 yr. We estimate from numerous simulations that the time of closest approach is probably anywhere from $1\text{–}8 \times 10^7$ yr, with a likely value around 4×10^7 yr.

3.2. *Summary of Fit to IC 2163*

Figure 4 reproduces most of the important observed features of IC 2163. It does not do a particularly good job of reproducing the tidal arm on the companion side (the western tidal arm), probably because the companion is approximated to be a point mass.

The main features of IC 2163 reproduced by the model are the following. (1) The ocular structure with a sharply pointed oval and tidal arms smoothly continuing off from the oval sides (compare to the optical images of IC 2163 in § 2 of Paper I). (2) The arm on the anticompanion side has a double-parallel structure with the right length, width, pitch angle, and orientation relative to the oval (see § 2 in Paper I). Notice the improved fit to the width of the H I streaming arm as compared to the ESES models (see § 4.2 in Paper I). (3) The interarm region on the concave side of the anticompanion tidal arm is nearly devoid of stars because of the clearing action of the tidal response (see § 6.1 in Paper I). (4) The inner region in the oval appears to have a bar that is oriented vertically in the figure, i.e., along the minor axis of the oval and the major kinematic axis (see §§ 2 and 4.3 in Paper I). This density feature is not a true bar in the deprojected image, which is shown in Figure 4; it is only an offset and asymmetric nucleus that has been made to look like a bar by the projection. (5) The nucleus is not in the center of the oval but is displaced toward the inside of the arc of the eastern tidal arm (see Fig. 1*a* in Paper I). (6) The kinematic minor axis (160° counterclockwise from vertical in Figures 4 and 5) is nearly perpendicular to the photometric minor axis, which is the minor axis of the oval (see § 4.3 in Paper I). This is the key observation of IC 2163 that demonstrates that the oval is intrinsic to the disk and not an artifact of projection. The intrinsic oval shape of the inner region is clearly seen in the unprojected version in Figure 2. (7) The line-of-sight velocity is nearly constant along the outer extension of the tidal arm (see § 4.3 in Paper I). (8) The velocity on the streaming part of the double-parallel tidal arm is higher than the velocity on the tidal arm part (see § 4.2 in Paper I). (9) The velocity contours (Fig. 5) have C-shaped deviations on the eyelid regions of the ovals, with the correct orientations, resulting from prograde streaming motions along the oval (see Fig. 11 in Paper I). (10) The time since the closest approach is $1\text{–}8 \times 10^7$ yr in various models, suggesting that the actual time was $\sim 4 \times 10^7$ yr for IC 2163, which places this galaxy in the proper position relative to NGC 2207, considering the orbit discussed in § 2. The companion is indicated in Figure 2.

4. NGC 2207

4.1. *Model*

The most striking feature of the velocity field of NGC 2207 is the warp throughout the whole disk (see Fig. 20 in Paper I). This suggests that IC 2163 perturbed NGC 2207 perpendicular to the plane, so we ran models with this type of interaction. The models were constructed with 30 equally spaced radial increments, or rings, and 30 equally spaced angular sections in each ring. The surface density and circular rotation speed in each section was specified at the beginning of the simulation, and a symmetric perpendicular acceleration of the form (Hunter & Toomre 1969)

$$A_{z,\,\mathrm{tidal}}(x, y) = \frac{1.5GM_c\, r \cos(\theta - \theta_c) \sin(2b_c)}{r_c^3} \qquad (2)$$

was applied (the factor of 1.5 comes from Hunter & Toomre's eq. [61]). Here x and y are coordinates in the plane of NGC 2207, $r = (x^2 + y^2)^{1/2}$ is the distance to the coordinate axis, $r_c = (x_c^2 + y_c^2 + z_c^2)^{1/2}$ is the distance to the companion, which has coordinates (x_c, y_c, z_c), $\theta_c = \arctan(y_c/x_c)$ is the azimuthal angle of the companion relative to the $y = 0$ axis of the coordinate system, $\theta = \arctan(y/x)$ is the azimuthal angle of the

point in the disk, and $b_c = \arctan [z_c/(x_c^2 + y_c^2)^{1/2}]$ is the latitude of the companion viewed from the center of the disk. The companion mass, M_c, was taken to be equal to the galaxy mass (to be consistent with our models for IC 2163).

The self-gravitational restoring acceleration in the perpendicular direction in the disk was determined by a direct summation of the accelerations from all pairs in the disk, using the symmetry in the accelerations to save computer time. The equation for this acceleration is

$$A_{z,\,\mathrm{self}}(x_i, y_i) = \sum_j \frac{G\,dM_j(H_j - H_i)}{[(x_i - x_j)^2 + (y_i - y_j)^2 + (z_i - z_j)^2]^{3/2}}\ , \tag{3}$$

where dM_j is the mass in the cell at position (x_j, y_j) and H is the height above the midplane. The heights and perpendicular velocities were changed with time according to the equations $dH/dt = -\Omega\, dH/d\theta + v_z$ and $dv_z/dt = -\Omega\, dv_z/d\theta + A_{z,\,\mathrm{tidal}} + A_{z,\,\mathrm{self}}$ for angular rotation rate Ω. The time step was varied at each step according to a Courant condition.

The disk was taken to be exponential with a disk scale length r_{disk} equal to 0.25 times the total disk radius (the total disk radius is comparable to $R_{25} = 22$ kpc for NGC 2207) and a central surface density of 500 $M_\odot$ pc^{-2}. The rotation curve was taken to be of the generic form

$$V(r) = \frac{V_0\,\xi}{\xi^A + \xi^{1-\alpha}}\ , \tag{4}$$

where $\xi = \xi_0\, r/r_{\mathrm{disk}}$ for constant ξ_0, which determines how rapidly the rotation curve rises in the central part, and for constants $A = 0.1$ and $\alpha = 0$, which determine the overall shape of $V(r)$. The characteristic velocity was taken to be $V_0 = 230$ km s^{-1}, considering the overall velocity field of NGC 2207. For the most realistic fit to the warp, ξ_0 was taken to be equal to 3. This form for the rotation curve is typical for real galaxies, but it is not consistent with the exponential disk; as usual, we assume that the rotation curve results partly from the disk and partly from an invisible halo.

A variety of parameters for NGC 2207 and a variety of trajectories for the companion were run. All the results shown here are for a parabolic companion trajectory. The distribution of heights H and perpendicular velocities v_z in the disk were saved at regularly spaced time intervals. Then the vector-combined (rotation plus z) line-of-sight velocities were displayed as gray-scale images and contours with various projections and orientations in the sky, for comparison with the observed velocity distribution in NGC 2207, from Figure 20 in Paper I. The displayed projections also considered the warp that resulted from the distribution of disk height H.

For all companion trajectories, whether perpendicular to the plane of NGC 2207 or parallel and offset from the plane, the basic reaction to the perturbation always has a characteristic feature: initially, there is a near-equilibrium distribution of heights and z velocities that resembles a warp when the companion is far away and the tidal force does not change rapidly. This warp is such that the perpendicular acceleration is largest at the azimuthal angle nearest the companion, so that the perpendicular velocity is largest downstream from this angle, carried by the rotation of the galaxy, and the perpendicular displacement H is largest downstream from this position of maximum v_z, again because of rotation. This near-static distribution in z then changes suddenly when the companion either crosses through the extrapolated plane of the disk or crosses over from one side to the other of the disk [i.e., when $\cos(\theta - \theta_c)\sin(2b)$ changes sign]. In effect, the z distribution attempts to find a new equilibrium with the companion on the other side, but because of the self-acceleration, $A_{z,\,\mathrm{self}}$, there is instead a dynamic response to the change in $\cos(\theta - \theta_c)\sin(2b)$ that consists of a rapid rotation and shear of the z perturbation that leads to a spiral-like shape in z, with the z velocity and height H still $\sim 90°$ out of phase, but now along a trailing spiral distribution (which is not a density wave but a z wave). This z spiral propagates inward toward the nucleus, and it either enters the nuclear region, possibly leaving the nucleus with a slight tilt, or it reflects off the inner disk and avoids the nuclear region, depending on the rotation curve (steep inner rotation curves allow the z perturbation to go further into the nuclear region). After the spiral moves in as far as it will go, it propagates outward with ever-decreasing wavelength because of the decreasing mass surface density with radius. This outward propagation and shortening of wavelength was discussed by Hunter & Toomre (1969).

An example of the z-spiral evolution that has the parameters of the preferred model for NGC 2207, discussed later, is shown in Figures 6 and 7. In all the figures displaying models for NGC 2207, the outermost radius is R_{25}. Figure 6 shows the z velocities at 20 time steps from -4.5×10^8 yr in the top left, increasing from left to right and then down the page, to a final time step of 5×10^8 yr in the bottom right, in time steps of 5×10^7 yr. The time of closest approach occurs at the tenth frame, which is second from the left in the third row. The rotation curve of the galaxy has $A = 0.1$, $\alpha = 0$ and $\xi_0 = 3$, as shown in Figure 8.

The gray scale in Figure 6 is black for velocities that are away from us, into the page, and white for velocities that are toward us, or out of the page. Each frame is separately normalized to give the maximum contrast gray scale, linear in v_z, for the purposes of emphasizing the z structure. The actual z velocities to which these frames are normalized vary from frame to frame. Figure 9 shows the maximum z velocity (as a solid line) as a function of time in this run.

Figure 7 shows the height distribution for the same time steps as in Figure 6. Again, each frame is normalized to maximize the contrast. Black represents z displacements into the page, and white is out of the page. The maximum height reached by the deformation is shown as a function of time as a dashed line in Figure 9.

The companion galaxy (a point mass) for the model in Figures 6 and 7 moves in a parabolic orbit with an orbital plane perpendicular to the initial disk of the model and with a 15° tilt between the radius vector to the pericenter position and the galactic spin vector. (A wide range of inclinations was run, but this perpendicular case fit the observations best.) This orbit is drawn from various perspectives in Figure 10, in which each dot shows the companion position at one of the frames in Figures 6 and 7 (i.e., separated by time steps of 5×10^7 yr). The time sequence starts with the small dots and ends with the large dots; the first large dot is at perigalacticon. (In this figure, the disk of the model galaxy is drawn as intrinsically circular with radius R_{25}; the galaxy outline shown in Figure 10 does not match the outline of NGC 2207 because Figure 10 does not account for the warp.)

The top left panel in Figure 10 shows the orbit in the reference frame of the model with the disk of NGC 2207 face-on, that is, from the same top-down perspective as the plots in Figures 6 and 7. In the top right panel of Figure 10, the plane

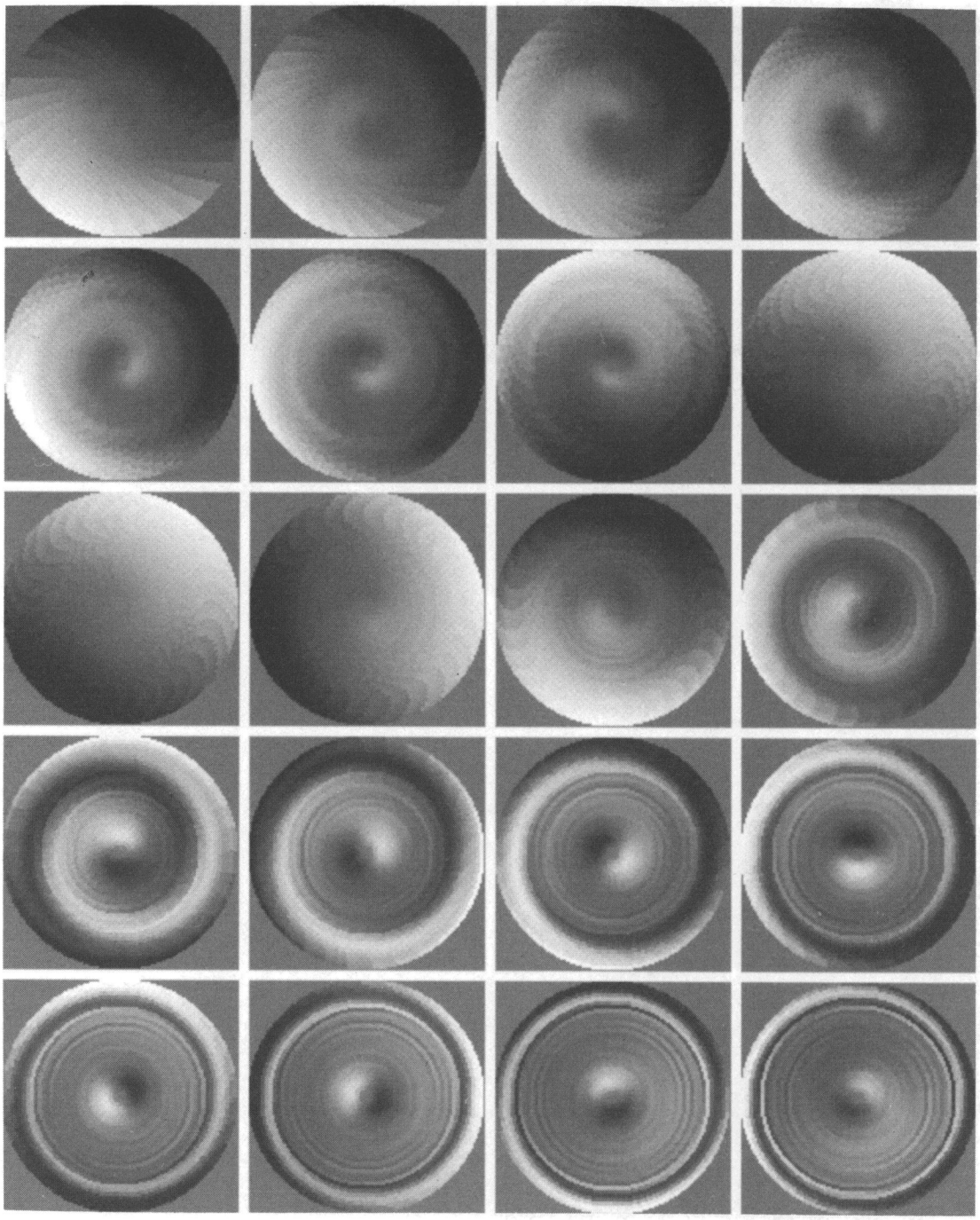

FIG. 6.—Twenty time steps in the evolution of the perpendicular velocity of an oscillating disk perturbed by an equal-mass companion galaxy with the orbit shown in Fig. 10 below. The disk rotates clockwise. The time steps start at −450 million years and increment in units of 50 million years, first across the page and then down row by row. Perigalacticon is in the 10th frame, and the preferred solution for NGC 2207, at 40 million years, is close to the 11th frame, which is third from the left in the third row from the top. Black shading represent velocities into the page. Each frame is normalized separately to give maximum contrast. The absolute velocities scale as in Fig. 9. A swirl in the pattern of perpendicular velocities is evident at various times.

of the paper is the orbital plane, made by inclining the top left figure 90° and then rotating it counterclockwise 90°. The bottom left panel shows the companion as a function of time for the preferred projection of NGC 2207, which is a counterclockwise rotation of 50° followed by a projection of 35°. The bottom right frame is a 50° counterclockwise rotation of the bottom left frame, to show the orientation of the orbit with north up in the figure.

In the model, the companion first crosses the plane of NGC 2207 at position $(x, y, z) = (0, -2.70, 0)$ times the galaxy radius. This occurs at time -2.0×10^8 yr, which corresponds to frame 6 in Figures 6 and 7, and to the sixth small dot from the end in Figure 10. Then, the companion moves behind the model galaxy and reaches a perigalacticon of $(x, y, z) = (0, 0.26, -0.96)$ at time zero. At the preferred value of 4×10^7 yr for the present time, the companion is just to the right of the second

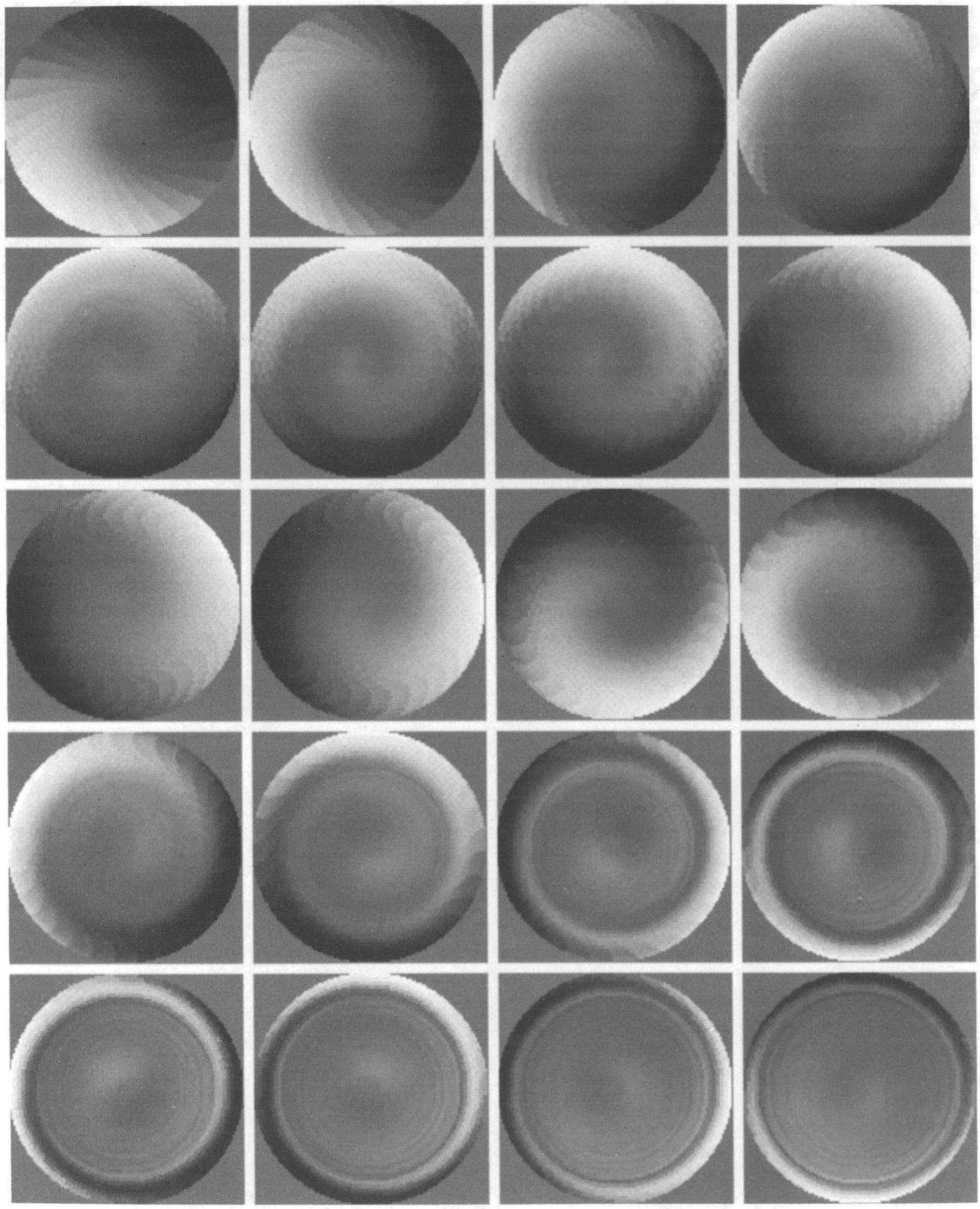

FIG. 7.—Twenty time steps in the evolution of the perpendicular height of the oscillating disk shown in Fig. 6. Black shading represent displacement into the page, with each frame normalized to optimize contrast; the maximum heights in each frame are plotted in Fig. 9 below.

large dot near the middle of the orbit in the top right panel of Figure 10. Notice how close the companion comes to the disk. The companion subsequently crosses the disk plane at position $(x, y, z) = (0, 1.57, 0)$ times the galaxy radius and at a time of 8.8×10^7 yr (this has not yet happened in the real system). This second plane crossing occurs between frames 11 and 12 in Figures 6 and 7.

The twist in the observed velocity distribution in NGC 2207 resembles the open z spiral in Figure 6 that appears shortly after the companion crosses the meridian, which is the horizontal line through the nucleus (i.e., near frame 11). The exact pattern for NGC 2207 is not apparent in this figure because the plotted time steps are too large. To get a better fit to the observations, we considered output time steps of 2×10^7 yr. (This output time step is not the same as the integrating time step for the simulation, which is more like 10^3 yr, varying with each step.)

The relation between the z spiral in the model and the velocity distribution in NGC 2207 is not obvious until the model is viewed in projection and with the model plane actually

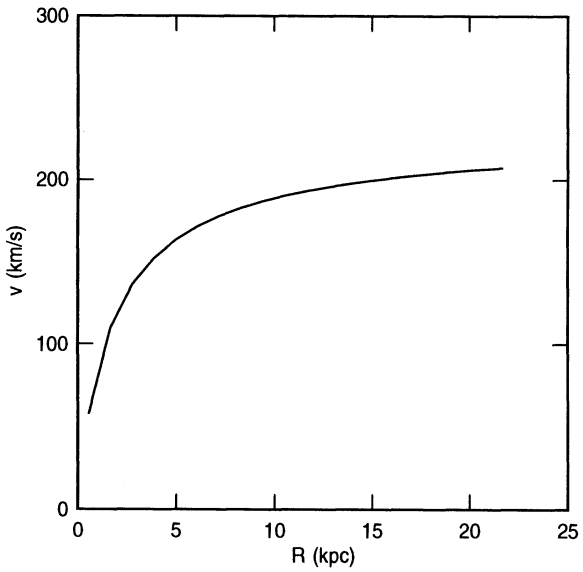

FIG. 8.—Rotation curve for the best-fit model of NGC 2207

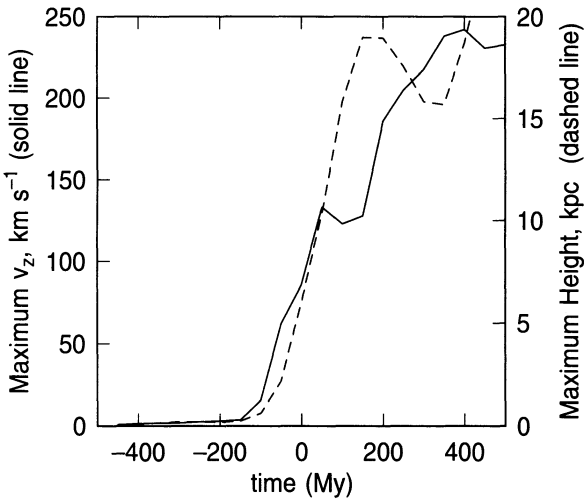

FIG. 9.—Maximum perpendicular velocities and heights as a function of time for the model shown in Figs. 6 and 7. At the epoch of the IC 2163/NGC 2207 collision, which is at 40 million years on this diagram, the maximum perpendicular velocity of the warp is 120 km s^{-1}, and the maximum displacement is 9.3 kpc.

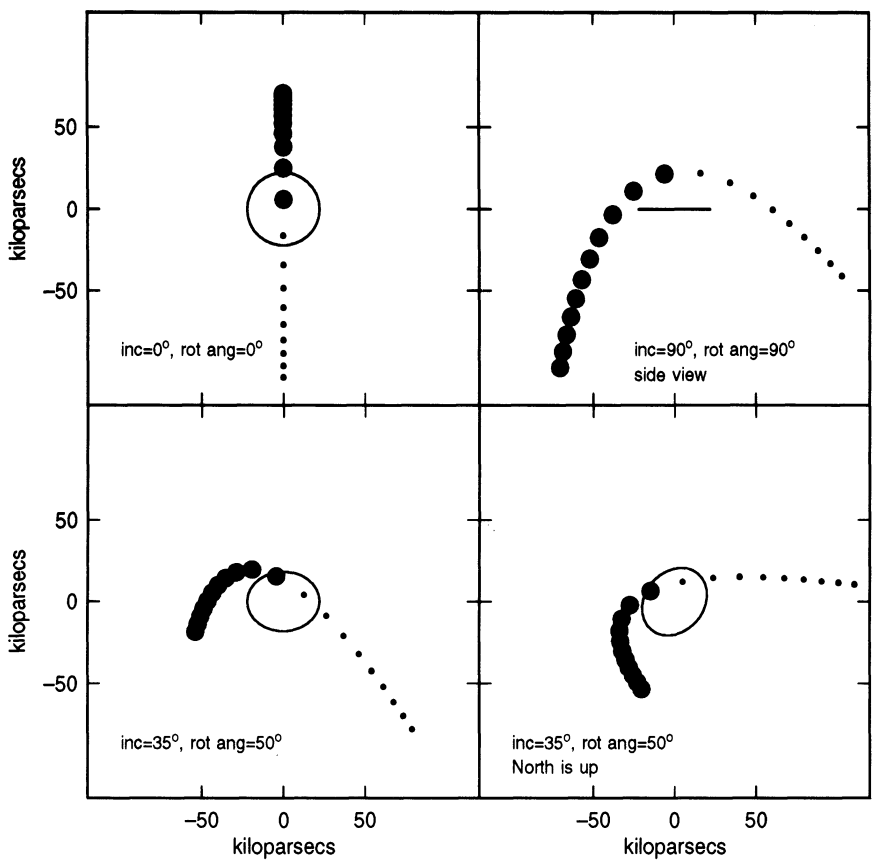

FIG. 10.—Trajectory of the companion galaxy in the model of NGC 2207, at the time steps shown in Figs. 6 and 7. The four frames show different projections: at the top left is the projection in the model coordinates, looking down the z axis in the same sense as in Figs. 6 and 7; at the top right is in the orbit plane; in the bottom left is the preferred projection for NGC 2207 made by rotating the model coordinates 50° counterclockwise and then inclining the model 35° with the top part out of the page; the bottom right frame twists the bottom left frame 50° counterclockwise to make the path of the trajectory resemble that of IC 2163 with north up in the figure.

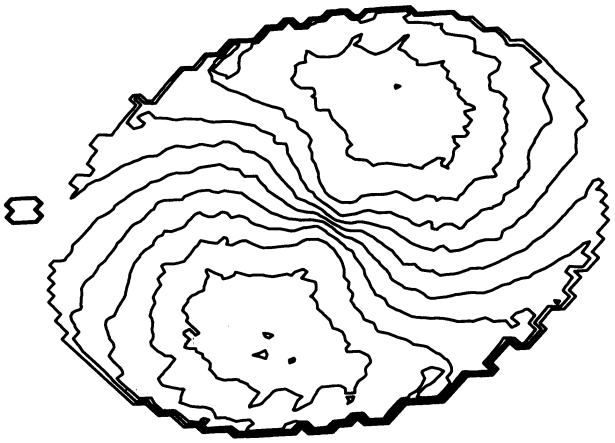

FIG. 11.—Velocity contours for the perpendicular collision model shown in Figs. 6 and 7 at the time, 40 million years, when they most resemble the line-of-sight velocity distribution in NGC 2207.

deformed by the height distribution. A typically good fit to the observations is shown as a velocity contour diagram (20 km s^{-1} contour interval) in Figure 11. This is for a time of 4×10^7 yr in the model shown in Figures 6 and 7.

The steps that were necessary to make Figure 11 are shown in Figure 12. At the top left and right of Figure 12 are the v_z and height patterns at the time step of 4×10^7 yr, with the same convention for white and black as in Figures 6 and 7. The small plus sign outside the galaxy is the position of the companion. In the middle row (*left*) is the v_z pattern after rotation of the model coordinate axes counterclockwise by an angle of 50°. In the middle row (*right*) is the line-of-sight velocity for this same rotation, made by inclining the galaxy 35° around a horizontal axis in the figure. This means that the major kinematic axis is horizontal in the figure. The inclination is such that the top part of the galaxy is out of the page, toward us. Black is still for motions that are away from us. Now most of the observed velocity pattern is from the rotation curve shown in Figure 8, but this rotation curve is distorted by the z component of the plane's motion on the line of sight.

This middle right frame of Figure 12 is the velocity pattern that would be observed in a galaxy with this rotation curve and v_z distribution if the galaxy were not warped, i.e., if the stars were still in a plane. But the z motions also produce a warp, and so each pixel in the model really corresponds to a position in three-dimensional space. The frame on the bottom left in Figure 12 shows the line-of-sight velocity pattern that arises when the (x, y, z) positions of the model pixels are all projected with the 50° counterclockwise rotation and 35° inclination, using for the z values the calculated height distribution as a function of x and y. Now the warp manifests itself by making the projected ellipse of the galaxy disk tilted at an angle relative to the major kinematic axis, which is still horizontal. The parts of the disk with the maximum and minimum line-of-sight velocities are still close to the kinematic major axis, but these parts are offset from the apparent major axis of the warped ellipse by a relatively large angle, ~40°. We believe that this offset is what makes the apparent major and minor kinematic axes in NGC 2207, shown in Figure 20 of Paper I, offset from the major and minor photometric axes of the optical disk, shown in Figure 1 of Paper I. The height distribution in the warped disk at this time step is shown on the bottom right of Figure 12.

Figure 11 shows the contours from the projected velocity distribution from the bottom left of Figure 12. These contours and the overall configuration of the galaxy and the companion resemble the observations of NGC 2207. To orient the model results relative to the sky coordinates for NGC 2207, the model in Figure 12 was twisted counterclockwise by 50° to make Figure 11. Thus 50° + 90° = 140° is the true position angle for the projection line of nodes of the central disk of NGC 2207.

4.2. *Summary of Fit to NGC 2207*

The model in Figure 11 fits the observations of NGC 2207 in several ways: (1) the elliptical shape of the optical image of NGC 2207 is reproduced with the companion IC 2163 at the proper position relative to the ellipse; (2) the overall magnitude of the rotation speed in NGC 2207 is reproduced (both Fig. 20 in Paper I and Fig. 11 here have the same 20 km s^{-1} contour values); (3) the warp in the velocity distribution is reproduced, with the kinematic major axis at the correct position angle relative to the photometric major axis, and (4) the S-shaped velocity contours throughout the main disk are reproduced.

The model also gives (5) about the same time since the first plane crossing in the west-northwest of NGC 2207 that was estimated from the morphology of the southern H I extension, considering our assumption for the most likely rotation curve. In the model, this time is the difference between the epoch of the preferred solution for NGC 2207, which is about 4×10^7 yr, and the time of the first plane crossing, which is -2.0×10^8 yr, giving about 2.4×10^8 yr from the first plane crossing to the present epoch. We commented in §§ 2 and 5 how this first plane crossing could have made the southern extension seen in H I.

In addition, the model for NGC 2207 gives the following: (6) about the same time since the closest approach to the companion as did the models for IC 2163; in the model for NGC 2207, the preferred fit time is 4×10^7 yr from closest approach, based on the twist in the velocity distribution. This time is uncertain and, in runs with different parameters, ranges from about 2×10^7 yr to 6×10^7 yr. After this time, the z spiral wraps up too much, depending on the rotation curve. The timing for NGC 2207 is more precisely determined from the position of the companion for an assumed orbit, but since the pericenter distance is not known (in the models for Figs. 6 and 7 it was assumed to be 1.0 times the circle radius), we could have chosen a larger pericenter distance to slow down the interaction (with other adjustments, mostly unreasonable, to give about the same velocity distribution as in the preferred model). Recall that for the IC 2163 models, the time since the closest approach was 1–8 $\times 10^7$ yr, which is close enough to the 4×10^7 yr for the NGC 2207 model to be an acceptable fit.

One interesting implication of this model for NGC 2207 is that the line of nodes for the tilt in the disk is not parallel to the major optical axis, but more parallel to the kinematic major axis (on the bottom left in Fig. 12, the line of nodes is exactly horizontal, and the kinematic major axis is approximately horizontal too). Considering the orientation of the model, we conclude that the line of nodes in the main disk is at a position angle of 140°. This implies that whereas the northern part of the disk of NGC 2207 is tilted toward us with the general inclination of the galaxy, the northwest part is bent or curved slightly more toward us because of the warp in the disk. This relative bend or warp is about 9 kpc perpendicular to the average disk (see Fig. 10). Similarly, the southern part of NGC 2207 is generally farther from us than the nucleus because of

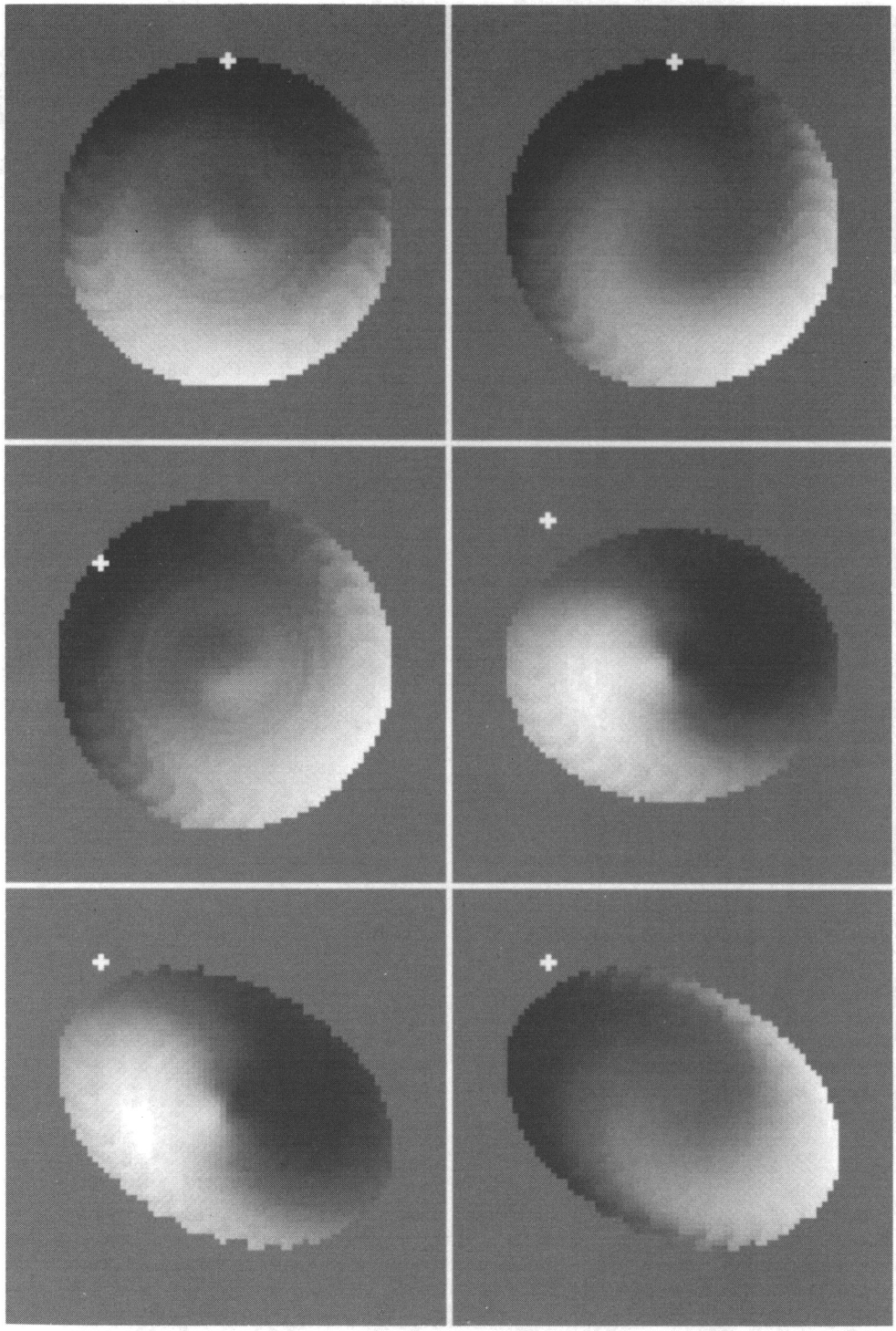

FIG. 12.—Six frames showing how Fig. 11 was made, as discussed in § 4

the general inclination, but the southeastern part (closest to IC 2163) is curved away from us even more relative to this tilt because of the warp.

The proximity of the southeastern part of NGC 2207 to IC 2163 may have caused the high-velocity filament seen as a perpendicular interloper on the eastern tidal arm in the velocity map of IC 2163 (Fig. 12 in Paper I) to have accelerated away from us toward IC 2163, giving this filament the observed peculiar high velocity.

The distance between the nuclei is currently about 22 kpc, according to the model. Because the southeastern side of NGC 2207 is bent toward IC 2163 in the warp, material from the western tidal arm of IC 2163 may be accreting onto NGC 2207. Gas accreted from the tidal bridge may be contributing to the

apparent shock front on the eastern side of the ring in NGC 2207, observed as a radio continuum ridge (see § 7.1 in Paper I).

The distribution of path lengths through the disk resulting from the tilt of the plane relative to our line of sight is shown in Figure 13. This figure was made by counting the number of cells in the original face-on model image that overlap in the final projected image at the bottom of Figure 12. The display in Figure 13 is darkest in areas where the disk is crossed twice by the line of sight, although the contrast has been enhanced to show the pattern. The maximum fold along the line of sight occurs near the isophotal minor axis at the edge of the main disk; here, the line of sight passes through about twice as much material as on the isophotal major axis. This is not the position of the main warp, which is closer to the major axis according to the bottom right panel in Figure 12. The warp puts more of the curvature into the line of sight on the isophotal minor axis than on the isophotal major axis. Thus, the fold along the line of sight produces limb brightening on the northern and southern parts of the ring. These are the portions observed to be the faintest, so the projection effects must exaggerate the ringlike appearance of the H I, in which case the eastern and western parts of the ring would have to be intrinsically bright.

Figure 13 here should be compared with Figure 17 in Paper I. If we take the lowest level H I contour in Figure 17 of Paper I as marking the edges of the H I ring, we see that the isophotal major axis at the outside edge has a P.A. of 100°, but the isophotal major axis of the inside edge appears to be roughly at 140°. Such a change in major axis position angle is expected in the above model but may also have been influenced by the bar.

There are many unknown parameters in these solutions, but most plausible combinations of parameters were found to give unacceptable fits, thus narrowing the range of possible solutions to be close to the ones we have shown here. The unknowns are the relative masses of the galaxies, the rotation

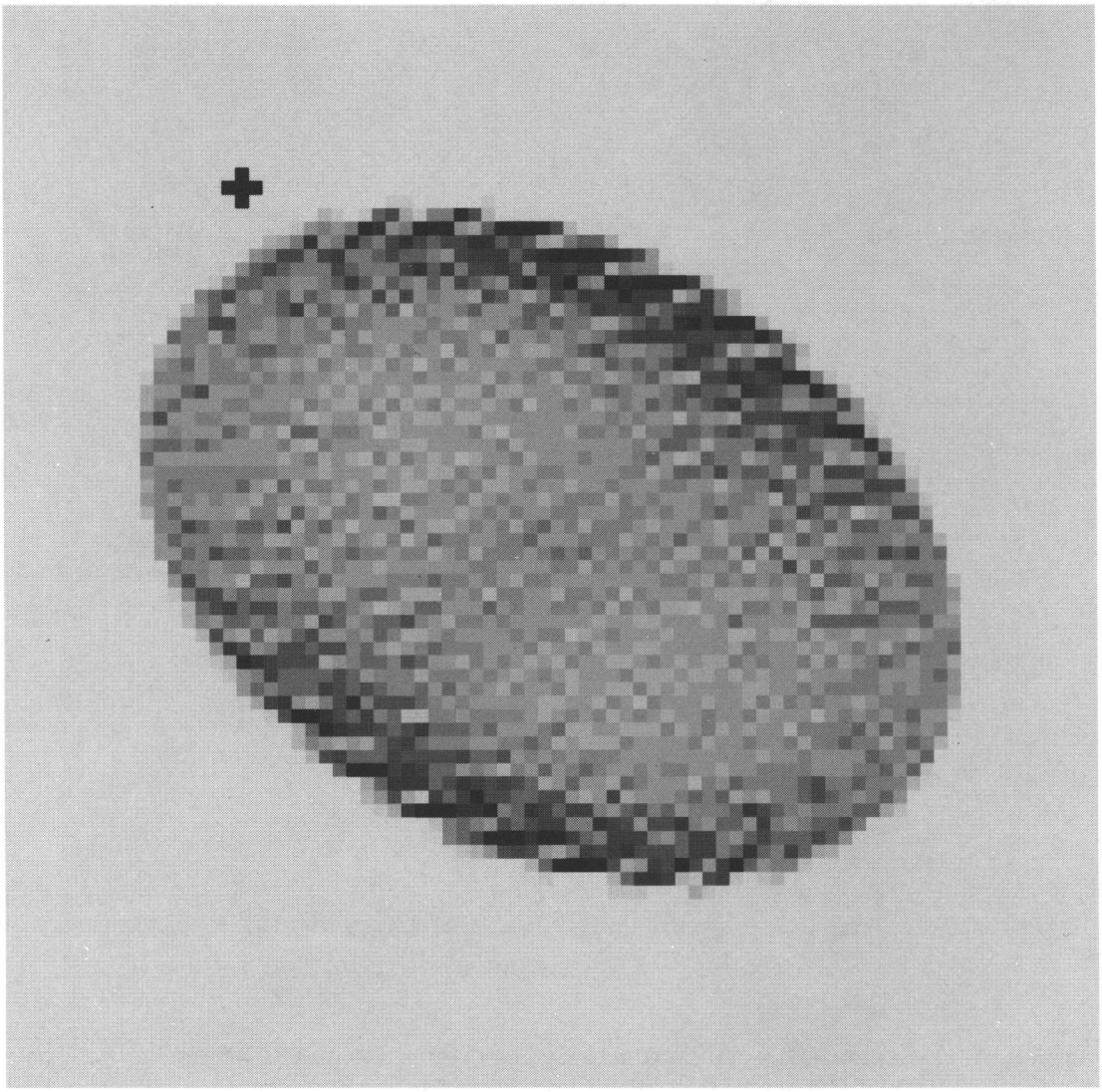

FIG. 13.—A gray-scale representation of the number of line-of-sight crossings of the model galaxy disk in the projection preferred for the NGC 2207 fit. In the darkest regions, the model galaxy curves back on itself because of the perpendicular warp, and the plane is crossed twice by the line of sight. The orientation here is the same as in the bottom left frame of Fig. 12. The position of the companion is shown by the cross. The gray scale is enhanced in the sense that it is proportional to the fourth power of the number of fractional model cells that contribute to each position on the line of sight. The bending effect is most noticeable on the minor axis, although the perpendicular displacement is largest closer to the major axis, as shown by the bottom right frame in Fig. 12.

curve of NGC 2207 (because of the twist, the true rotation curve cannot be observed directly), the entire orbit history of the companion (aside from the broad constraint that the interaction for IC 2163 was probably prograde and in-plane), the time since closest approach, and the true inclination and intrinsic shape of NGC 2207. We experimented with all of these parameters in several hundred trials with many disk orientations per trial. All of the acceptable fits had parameters that clustered around those chosen for Figure 11. For example, different companion orbits changed the timing and the relative positions of the companion, and this, along with the constraints from the ocular structure in IC 2163 and the southern extension, helped narrow down the preferred orbit. Different companion masses changed the amplitude of the z response, making the twist more or less pronounced. Different rotation curves changed the shape of the contours at the acceptable times, although curves with ξ_0 equal to 2, 3 or 4 were all acceptable (Figure 11 has $\xi_0 = 3$, which seemed the best). Different A and α for the rotation curve did not have much effect unless they were greatly different from the chosen values, but then the intrinsic rotation curves looked unrealistic. Different inclinations changed the elliptical shape of the NGC 2207 model and the relative position of the companion at the preferred time, as well as the shape of the velocity contours.

5. CONCLUSIONS

The morphology, orientation, internal kinematics, and positions of each galaxy imply the following orbit. IC 2163 crossed the extrapolated plane of NGC 2207 in the west $\sim 2.4 \times 10^8$ yr ago, and this disk crossing tidally stretched the nearby portion of the NGC 2207 disk and turned it into the southern extension after one-fourth of a rotation. The expansion caused the southern extension to be intrinsically elliptical, with a line of nodes different from that of the main disk. It probably also deviates from the main plane of NGC 2207. The filaments in the southern extension have the correct pitch angle for the expected radial and azimuthal motions of this gas. After this disk crossing, IC 2163 proceeded in its orbit to the backside of NGC 2207, where it reached perigalacticon $\sim 4 \times 10^7$ yr ago. Since IC 2163 traveled parallel to its own disk as it moved, NGC 2207 remained close to the plane of IC 2163. The large tidal forces at perigalacticon initiated the ocular structure in IC 2163 and most of the velocity warp in NGC 2207. It is clear from Figure 1 that with this orbit, the center of mass of NGC 2207 moved prograde (counterclockwise) relative to the disk of IC 2163 and in the plane of IC 2163, as required. Also, the center of mass of IC 2163 moved primarily perpendicular to the disk of NGC 2207, which is required to produce the S-shaped warp in the velocity field of NGC 2207.

Our observations and modeling of the galaxy pair IC 2163/NGC 2207 provide a view of the early stages of postencounter evolution. Many unusual features in these galaxies are fitted by the models in a self-consistent way:

1. The odd morphology of IC 2163 (i.e., the ocular structure with a strong, sharply pointed oval and a double-parallel tidal arm on the anticompanion side) and the velocity anomalies (i.e., the streaming motions along the oval and the velocity difference between the two parts of the double-parallel tidal arm, as well as the perpendicular displacement between the kinematic and photometric minor axes in the oval) match the simulations of IC 2163 with an in-plane prograde encounter at close range. Other matches to features in IC 2163, including the apparent bar, were summarized in § 3.2.

2. The unusual 40° displacement between the kinematic and photometric minor axes and the pervasive S shape to the velocity field in NGC 2207 are matched by a moving, twisting warp that results from strong out-of-plane tidal forces exerted on NGC 2207 by IC 2163. This warp directly produces the S shape in the velocity contours, which is a well-known effect (e.g., Bosma 1981), but it also changes the elliptical outline of the projected disk so that it is still elliptical but at a relatively large angle (40°) from the line of nodes. Currently, the extent of the warp is about 9 kpc at the edge, where the radius is 22 kpc. The present perpendicular motions in the disk reach a maximum value of about 100 km s^{-1} near the edge.

3. The orbits brought the two galaxies very close to each other—perigalacticon in the models is only about one galactic radius for NGC 2207—yet the galaxies did not coalesce. This is an unusual situation, leading to strong but nondestructive tidal forces between these two massive galaxies. The nearby parts of the galaxies are probably falling toward each other and may actually be touching in parts: one of the filaments in the southern extension of NGC 2207 is moving at several hundred kilometers per second toward IC 2163 relative to the rest of NGC 2207 in that region, and the radio continuum ridge on the side of NGC 2207 closest to IC 2163 could be a shock front resulting from gas accretion from the nearby (optically obscured) tidal arm of IC 2163.

4. Both galaxy disks contain H I clouds with masses in excess of $10^8 M_\odot$. These are unusually large masses, a factor of 10 larger than the most massive clouds in normal galaxies. We suggested previously (Elmegreen et al. 1993) that they result from normal formation processes in the galactic disks, i.e., from local gravitational instabilities, but that the mass is large because of the unusually large velocity dispersions in the disk. Both IC 2163 and NGC 2207 have atomic hydrogen velocity dispersions in the range of 30 to 50 km s^{-1} (Paper I), whereas 10 km s^{-1} is normal. The large velocity dispersions are also likely to be the result of the strong tidal forces, as shown by numerical simulations in Elmegreen, Kaufman & Thomasson. The clouds are not forming stars in a burst, however; some of them contain only a modest amount of star formation, while others contain no evidence for star formation at all (Paper I).

This work was partially supported by National Science Foundation grant AST 92-01640 to D. M. E. and B. G. E. and by National Science Foundation grant AST 89-14969 to M. K.

REFERENCES

Barnes, J. E., & Hernquist, L. E. 1992, ARA&A, 30, 705
Bosma, A. 1981, AJ, 86, 1781
Donner, K. J., Engstrom, S., & Sundelius, B. 1991, A&A, 252, 571
Elmegreen, B. G., Kaufman, M., & Thomasson, M. 1993, ApJ, 412, 90
Elmegreen, D. M., Kaufman, M., Brinks, E., Elmegreen, B. G., & Sundin, M. 1994, ApJ, 453, 100 (Paper I)
Elmegreen, D. M., Sundin, M., Elmegreen, B., & Sundelius, B. 1991, A&A, 244, 52 (ESES)
Hunter, C., & Toomre, A. 1969, ApJ, 155, 747
Lynds, R., & Toomre, A. 1976, ApJ, 209, 382
Moles, M., Marquez, I., Masegosa, J., del Olmo, A., Perea, J., & Arp, H. 1994, ApJ, 432, 135
Persic, M., & Salucci, P. 1991, ApJ, 368, 60
Salo, H., & Laurikainen, E. 1993, ApJ, 410, 586
Smith, B. J., & Wallin, J. F. 1992, ApJ, 393, 544
Stanford, S. A., & Balcells, M. 1991, ApJ, 370, 118
Sundin, M. 1993, Ph.D. thesis, Chalmers Univ. of Technology, Göteburg, Sweden
Thomasson M. 1989, Res. Rep. 162, (Dept. of Radio and Space Sci. with Onsala Space Obs., Chalmers Univ. of Technology, Göteborg)